Internal Coordinate Couplings and Symmetry Properties: The Search of a Conical Seam in Protonated Oxygen

M. Ceotto and F. A. Gianturco*

Department of Chemistry, The University of Rome, Città Universitaria, 00185 Rome, Italy

Received: July 31, 2000; In Final Form: January 23, 2001

We show by a detailed computational experiment that the three-particle system of protonated oxygen allows us to study the behavior of curve crossings within the Born−Oppenheimer picture in terms of the relative strength of the couplings that exist between the relevant internal coordinates. In particular, we show that the one- and two-parameter seam found in the C_{2V} symmetry are reduced-dimensionality manifestations of an intersection that actually becomes a conical seam in the three-parameters C_s symmetry. We further show, then, that no trifurcation point exists in this case since the expected C_s seam of the AB_2-type systems does not appear in the O_2H^+ species.

I. Introduction

The protonated molecular oxygen, O_2H^+, is a very important moiety in many common chemical processes. The presence of the O_2H^+ has been detected so far only in ion−molecule reaction studies;[1−6] however, its importance is well-known in combustion processes, in plasmas reactions, and especially in the chemistry of the upper atmosphere (the ionosphere) where the solar wind and the earth magnetic field bring protons to react with oxygen.[7] The purpose of this work is "experimental" and theoretical at the same time: from the experimental point of view, we carry out the numerical assembly of the full 3D-potential energy surfaces (PESs) for the first two adiabatic roots and their complete conical seam to extract from it a deeper knowledge of the dynamical processes that are more likely to occur. From a theoretical point of view, we suggest a methodology to identify the topology of the crossings in different symmetry point groups and to detect the different nature of the symmetry-induced versus the electronically induced conical intersections.

To follow our aims, we decided to study as an example a simple protonation reaction in the gas phase:

$$M + H^+ \rightarrow [MH]^+ \qquad (1)$$

in which the projectile is H^+ and is made to collide with a target M, thereby eventually generating a bound complex $[MH]^+$. Subsequently, the bound complex is considered to be able to undergo the following dissociation processes:

$$[MH]^+ \rightarrow \begin{cases} M^+ + H & \text{dehydrogenation} \\ M + H^+ & \text{deprotonation} \end{cases}$$

We have chosen this rather special projectile because it has a nucleus that is much lighter than the partner oxygen molecule, it does not "add" electrons to the target, and, further, it is a ionic partner. Consequently, its special reactivity allows us to study the reactivity of the target molecule in a rather general manner: the proton charge interacts with the electronic clouds of the oxygen without any induced effects over its own structure, a feature that permits us to focus solely on the target and on a reactivity that can be generalized to other reaction partners.

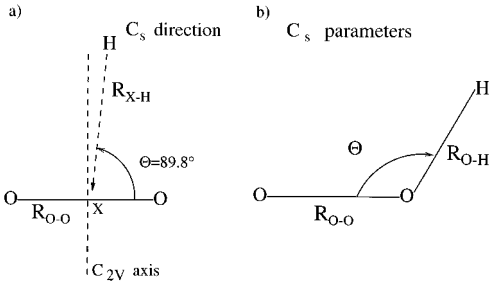

Figure 1. Representation of the coordinates adopted for the calculation of the PESs; (a) parameters for the C_{2V} PES and for the C_s 1D-PES next to symmetry axes; (b) parameters for the full PESs.

In the present work, we will therefore consider the following gas-phase protonation reactions:

$$O_{2(g)} + H^+_{(g)} \rightarrow [O_2H^+]_{(g)} \rightarrow \begin{cases} O_{2(g)} + H^+_{(g)} & \text{CT} \\ O_{2(g)}{}^+ + H_{(g)} & \text{ET} \end{cases} \qquad (2)$$

where the CT channel represents a "charge transfer" process in the sense that the protonated moiety $[O_2H^+]$ undergoes a deprotonation reaction, while the ET ("electron transfer") path represents the dehydrogenation process. Since the first ionization energy of O_2 is $E^{O_2}_{I.E.} = 12.0697\ eV$ and $E^{H_2}_{I.E.} = 13.5984\ eV$ for the hydrogen, the ET is energetically preferred by 1.5287 *eV*. We will however look at both channels and will find between them the phase-space point where it becomes most probable to follow the ET path, i.e., the MECP (minimum energy crossing point). Our aim here is to locate the coordinate physical region where such a point can exist, rather than to exactly pinpoint it.

As far as the computational part is concerned, we performed calculations using the second-order direct multiconfiguration method (MULTI) of Werner and Knowles[8−12] as available in the MOLPRO suite of programs with a cc-pVTZ basis set. We have used such basis set, which is relatively small as compared with previous calculations[13] performed on the same moiety, because our main purpose here, as mentioned above, is to show

* To whom correspondence should be addressed. Prof. F. A. Gianturco, Dipartimento di Chimica, Città Universitaria 00185 Rome, Italy. Fax: +39-6-49913305, E-mail: fa.gianturco@caspur.it.

10.1021/jp002748+ CCC: $20.00
Published on Web 05/05/2001

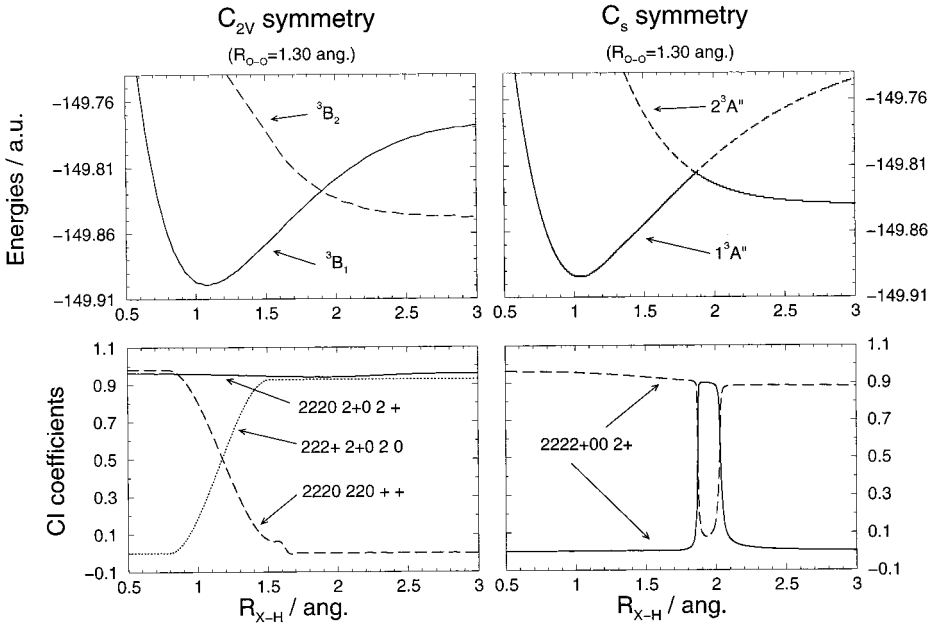

Figure 2. Unidimensional PES and relative CI coefficients; upper panel on the left: 1D-PES in C_{2V} symmetry; lower panel on the left: CI coefficients for the main configuration; upper panel on the right: 1D-PES along the C_s direction of Figure 1 for the first two interacting roots; lower panel on the right: CI coefficients of the main configuration for the two roots.

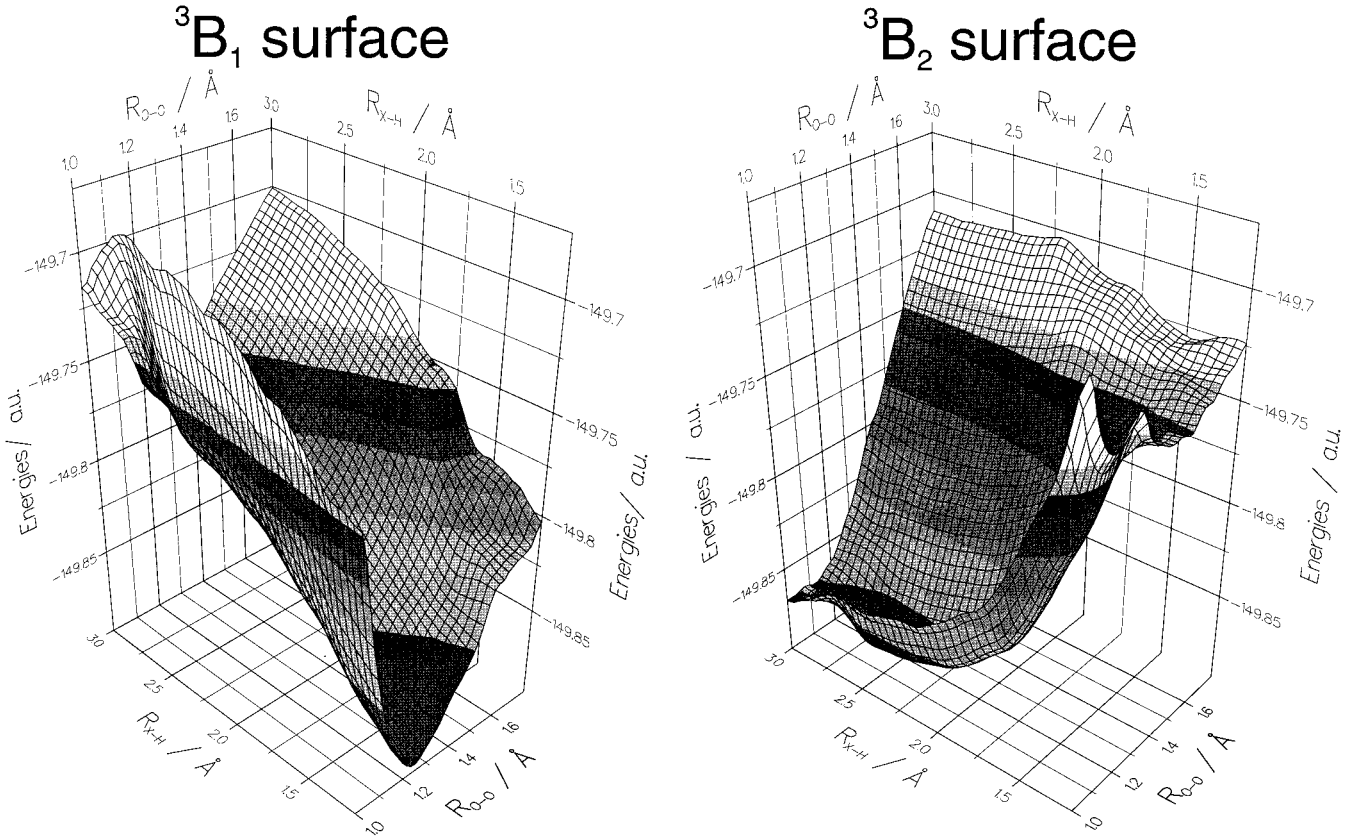

Figure 3. 2D-PES in symmetry C_{2V} for the two first roots.

that the conical topology of the crossing in the C_{2V} space is avoided in the C_s subspace. Such a proof does not depend on the choice of the basis set but rather on the symmetry features of the system. Furthermore, we did not calculate any spectroscopic features or any physical observable for which experiments might exist, but rather used only qualitative properties of the PESs from different symmetry groups. Concerning the ab initio method, we have found that the MULTI algorithm fits very well with the study of coupled adiabatic potential energy surfaces, as in our reaction, because the (SA-MCSCF) routine avoids root-flipping problems, and the convergence can also be achieved very close to the conical seam, as we shall show below. We have used about 850 CSFs which originally came from 2324 determinants and 4536 intermediate states. The orbitals space was divided into two parts, as is usual in a CASSCF calculation, which are the internal space (IS) and the external space (ES). The first one is then further divided into a close-shell orbital space, which was updated for each macroiteration, and into an

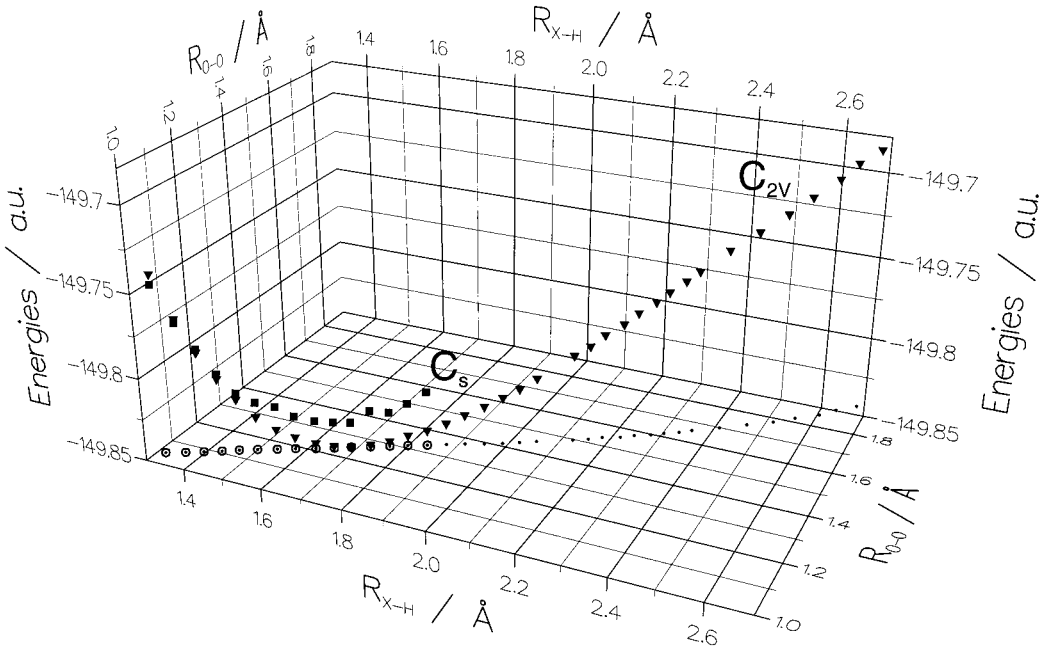

Figure 4. Schematic representation of the overlap between the PES of Figure 3. We represent with triangles the conical seam for the O_2H^+ molecule obtained from the C_{2V} symmetry curves crossings and with small dots its projection onto the parametric space; with squares we show the change of sign in C_s symmetry and with circles, its projection onto the 2D plane.

active-shell orbital space. For the calculations at the C_s symmetry of the system we used two closed-shell orbitals of IR (irreducible representations) A′ (2A′ 0A″) which are actually the 1s atomic orbitals of the two oxygen atoms, 9 active orbitals (7A′ 2A″), and 63 external orbitals (41A′ 22A″). For the C_{2V} geometries, we used instead two closed-shell orbitals ($1A_1$ $1B_1$ $0B_2$ $0A_2$), 9 active orbitals subdivided into ($4A_1$ $3B_1$ $1B_2$ $1A_2$), and a set of 63 external orbitals ($22A_1$ $19B_1$ $12B_2$ $10A_2$) from a total of 861 CSFs (1162 determinants and 4536 intermediate states) for the B_2 IR and 855 (1118 determinants and 4536 intermediate states) for the B_1 IR. For all the examined geometries, the O_2H^+ is given as an open-shell triplet state, a feature that will give rise to some problems concerning the sign change of the total wave function, as we shall further discuss below. We further fixed the ground state to be a triplet state according to the previous results,[13] although recent work has already shown that the singlet state A′ lies extremely close to the latter.[14] Neither choice is deemed to affect the finding of the present study.

To avoid this spurious change of sign, we forced our calculations to use the MCSCF state-averaged orbitals of the previous step, and therefore we did not encounter any spin-flipping problem.

In the following sections, we will briefly outline the nature of the geometric phase as it arises in the adiabatic approximation and will look at the conical intersections both from the electronic and symmetry points of view. We will then discuss the full PESs both in C_{2V} and C_s symmetries and the related MCSCF-wave function coefficients that allow us to localize the conical seam and shall conclude with a final discussion over the nature of the two types of conical intersections.

Symmetry and the Geometric Phase

The purpose of this section is to illustrate the origin of the geometric phase and its relation to the symmetry-breaking effects. The treatment reported here, without claim of originality, is discussed more extensively by ref 15. Let us take a generic Hamiltonian for the fast (**p**, **r**) and slow (**P**, **R**) variables:

$$H = \frac{\mathbf{P}^2}{2\mathrm{M}} + \frac{\mathbf{p}^2}{2\mu} + V(\boldsymbol{R}, \boldsymbol{r}) \tag{3}$$

and let us also define a reduced Hamiltonian governing the fast variables which depends parametrically on the slow ones.

$$h(\boldsymbol{r}, \mathbf{R}) = \frac{\mathbf{p}^2}{2\mu} + V(\mathbf{r}, \mathbf{R}) \tag{4}$$

Let $|n; \mathbf{R}\rangle$ be the eigenfunctions of the sub-Hamiltonian h (**r**, **R**), which are defined with less of a phase factor, with eigenvalues ϵ_n (**R**). We can then define the Berry's connection as

$$\boldsymbol{A}_n(\mathbf{R}) = \langle n; \mathbf{R}| i\nabla_{\mathbf{R}} |n; \mathbf{R}\rangle \tag{5}$$

and the "effective" Hamiltonian for the slow motion, in which the usual Born−Oppenheimer approximation allows the off-diagonal matrix elements $\langle n; \mathbf{R}| i\nabla_{\mathbf{R}} |n; \mathbf{R}\rangle$ to be ignored, reads

$$H_{\mathrm{eff}} = \frac{1}{2\mathrm{M}} (\mathbf{P} - \mathbf{A}_n(\mathbf{R}))^2 + \epsilon_n(\mathbf{R}) \tag{6}$$

Equation 6 shows that the fast system induces into the dynamics of the slow variables an additional PES ϵ_n(**R**) and a velocity-dependent interaction that arises from the Berry's connection $\mathbf{A}_n$(**R**). The effective Hamiltonian (6) is therefore seen to be invariant under gauge transformations that change **A** according to

$$\mathbf{A}\,(\mathbf{R}) \rightarrow g^{-1}\,(\mathbf{R})\,\mathbf{A}\,(\mathbf{R})\,g\,(\mathbf{R}) - ig^{-1}\,(\mathbf{R})\,\nabla g\,(\mathbf{R}) \tag{7}$$

and in the case where **A** (**R**) is an explicit function of **R** and g belongs to **U** (1), i.e., is given by $e^{i\theta}$, eq 7 reduces to the "electromagnetic" gauge transformation:

$$\mathbf{A} \rightarrow \mathbf{A} + \nabla\theta \tag{8}$$

which can be written as an infinitesimal transformation

$$\delta\mathbf{A} = \nabla\Theta - i\,[\mathbf{A}, \Theta] \tag{9}$$

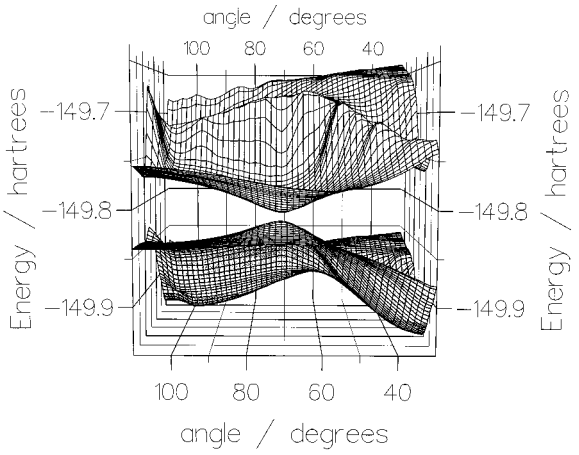

Figure 5. PESs for the first two roots and fixed $R_{O-O} = 1.30$ Å for different angles and R_{O-H} distances (shown by the depth of the box).

If the full Hamiltonian (3) possesses a symmetry, or, in other words, there is a constant of motion commuting with H, the symmetry will not be lost in the "effective" description, and there will be an "effective" constant of motion commuting with H_{eff}. If we take as an example the rotational symmetry, the associated angular momentum constant of motion is **J** and the orthogonal matrix of rotation is A.[15] Since the Berry's connection is rotationally invariant

$$\Lambda\mathbf{A}\,(\Lambda^{-1}\mathbf{R}) \rightarrow g^{-1}\,\mathbf{(R)}\,\mathbf{A}\,\mathbf{(R)}\,g\,\mathbf{(R)} - ig^{-1}\,\mathbf{(R)}\,\nabla g\,\mathbf{(R)} \quad (10)$$

and, taking into consideration the expression of an infinitesimal rotation of **R** which is

$$\delta\mathbf{R} = \mathbf{n} \times \mathrm{R} \quad (11)$$

we obtain the equation for the Berry's connection **A**:

$$\mathbf{n} \times \mathbf{A} - (\mathbf{n} \times \mathbf{R} \cdot \nabla)\,\mathbf{A} = \nabla\Theta - i\,[\mathbf{A}, \Theta] \quad (12)$$

which expresses, in infinitesimal form, the transformation of the vector potential **A** under a rotation around the axis **n**. Consequently, the conserved angular momentum $\mathbf{J} = \mathbf{n} \cdot (\mathbf{R} \times \mathbf{P})$ is supplemented by Θ, the gauge transformation generator, giving the following expression[15] for the "effective" angular momentum

$$\mathbf{J}_{\mathrm{eff}} = \mathbf{R} \times \mathrm{M}\frac{\partial\mathbf{R}}{\partial t} + \frac{\partial W}{\partial\mathbf{n}} \quad (13)$$

where

$$W = \Theta + \mathbf{n} \times \mathbf{R} \cdot \mathbf{A} \quad (14)$$

This means that the Born−Oppenheimer approximation induces in all phase space (**P**, **R**) not only that the total Hamiltonian H is modified with a gauge transformation into an "effective" one, but also that all constants of motion are accordingly modified. In a molecular system, the degeneracy can occur either because of its electronic structure or because of its symmetry properties. For a polyatomic system, the first case yields the degeneracy as an "electronically induced" conical intersection while the second case gives rise to a "symmetry induced" conical intersection.[16−18] The last one occurs, for example, when a system possesses C_{2V} symmetry, and, by varying one parameter to break its symmetry, it evolves from the B_1 and B_2 IRs into the A'' IR of the C_s symmetry, where the previous two IRs are now degenerate. Hence, one should encounter in the C_s symmetry phase-space an intersection between two A'' terms which is avoided in a one-dimensional C_s symmetry cut (because of the "avoided-crossing rule"[19,20]) and which has a conical topology in a multidimensional parametric space. We will show here how this is what actually occurs in the case of the protonated oxygen O_2H^+.

The Full PESs

We chose to gradually construct the full PESs by beginning with the 1D-PES and approaching the proton along the C_{2V} axes indicated on panel a of Figure 1. We fixed the parameter $R_{O-O} = 1.3$ Å which is approximately the equilibrium distance for the diatomic. Although we are chiefly interested in the ET process, and therefore we represent only the electronic terms of triplet spin symmetry for the first two roots of symmetry $^3B_1$ and $^3B_2$, we also calculated the other electronic terms, confirming with our calculations what had been found by the previous results.[13,14,21] The curves are represented in the upper panel on the left of Figure 2, where the ground electronic state $\tilde{X}^3B_1$ correlates with the asymptotic state $O_2(\Sigma_g^{3-}) + H^+$, while the upper electronic term $^3B_2$ correlates with the O_2^+ (Π_g^3) + $H(^2S)$. The next step for building the full PESs was to relax the interatomic distance R_{O-O} and calculate the 2D-PES of Figure 3. We chose a separate representation because the two multidimensional surfaces are of different symmetry and they can therefore overlap. On the left of Figure 3, we show the lower surface which exhibits a clear attractive shape with a minimum which we found to be at $R_{O-O} = 1.28$ Å and $R_{O-H} = 1.26$ Å. From Figure 3, we can guess a marked sensitivity of the PES regarding the variation of the parameter R_{O-O} versus that of R_{X-H}, showing therefore that the phase-space accessible to the molecule at a given energy is well confined in terms of the oxygen distance available. In other words, Figure 3 demonstrates that the large motion amplitude of the hydrogen atom versus the more limited one of the oxygen atoms gives us a first feature of the **R** subspace that turns out to be, as we shall see below, very important for the dynamics. To study the **P** space, we will need to further look at the MCSCF-CI coefficients, and we shall do it in the next paragraph. As far as the $^3B_2$ surface is concerned, we can see from Figure 3 that the extra energy of the system has been released to the molecular internal stretching since the PES is slightly wider than the previous one. Furthermore, if we fix $R_{O-O} = 1.60$ Å as an example of a larger distance then there is no noticeable variation of the second root curve for the different R_{X-H} values. This feature describes the fact that the proton is likely to cross the oxygen bond in its middle, without significant overlapping with the oxygen electronic clouds and without exchanging charge with them. The same happens for the first root, albeit at greater R_{O-O} distances that we cannot appreciate very well from the set of geometries shown by Figure 3.

If we imagine superimposing the two surfaces of Figure 3 to see only the set of degeneracy points, we will obtain Figure 4 where we represent these points with triangles in the same C_{2V} parametric space. We call (improperly) this line a "C_{2V} seam" because until now we have not demonstrated as yet the conical nature of these points. The seam was actually built by keeping the R_{X-H} crossing values from the unidimensional cuts of Figure 2 as calculated at each fixed value of R_{O-O}. We compute the seam points out to the largest parametric distances for which convergence of the MCSCF calculations was achieved, even if these points are not very important to understand the dynamics of the ET process. One important result of Figure 4, however, is to show the calculation of the MECP (minimum energy

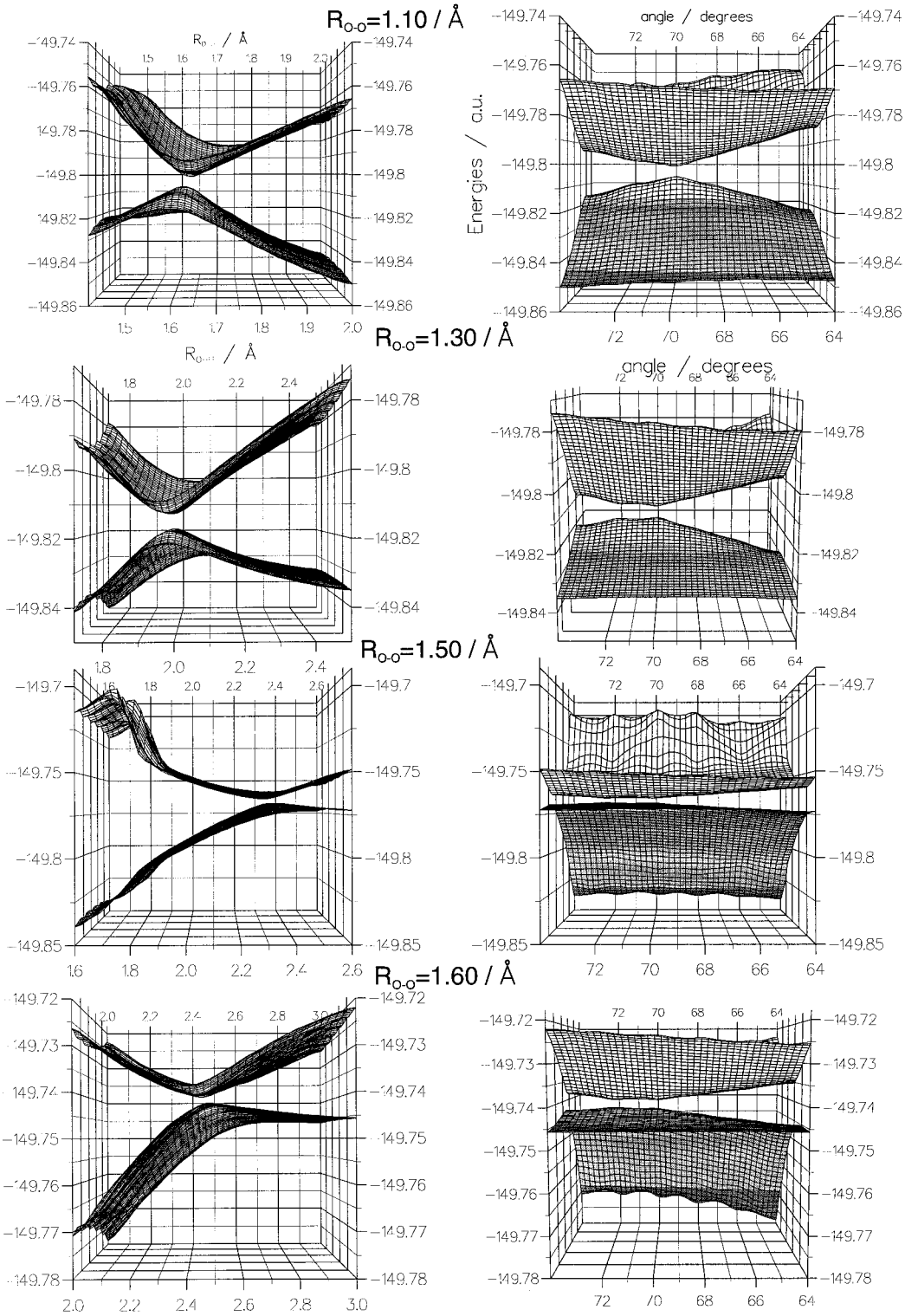

Figure 6. Computed PESs by varying all parameters: each panel shows different R_{O-O} values by showing the two projections onto the R_{O-H} and Θ subspaces.

crossing point) which is the point where the transfer of the electron from the oxygen molecule out to the proton is energetically the most probable. We assume from Figure 4 that the coordinates are $R_{X-H} = 1.70$ Å or $R_{O-H} = 1.82$ Å and $R_{O-O} = 1.30$ Å which is the value for the R_{O-O} equilibrium in the isolated molecule. For the R_{O-H} coordinate the values is far away from the local C_{2V} minimum: this shows again that the R_{O-O} distance is more or less constant during the dynamics. Furthermore, Figure 4 tells us that for large values of the R_{O-O} parameter the energy of the seam is fairly large and therefore the ET process is less probable. This occurs because the electronic clouds of the individual oxygens do not strongly overlap, and therefore the proton can travel between the two oxygens without "harpooning" an electron. For very short R_{O-O} distances, however, the seam moves again to high energy values (because of the proton-oxygen nuclear repulsion), and therefore it cannot approach the molecule close enough to extract the electron.

To complete the construction of the full PES, we further consider the parameters indicated in Figure 1, panel b. These

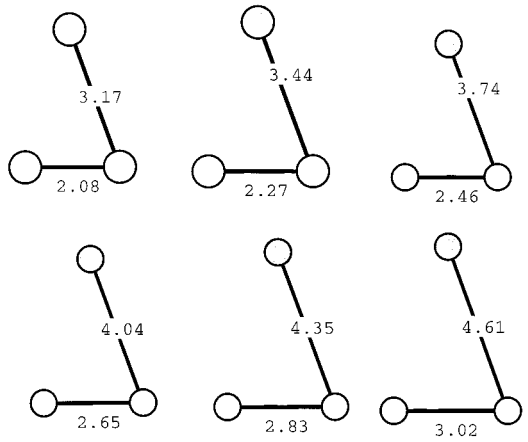

Figure 7. O_2H^+geometries at the degeneracies obtained from the parametric coordinates of Figure 6.

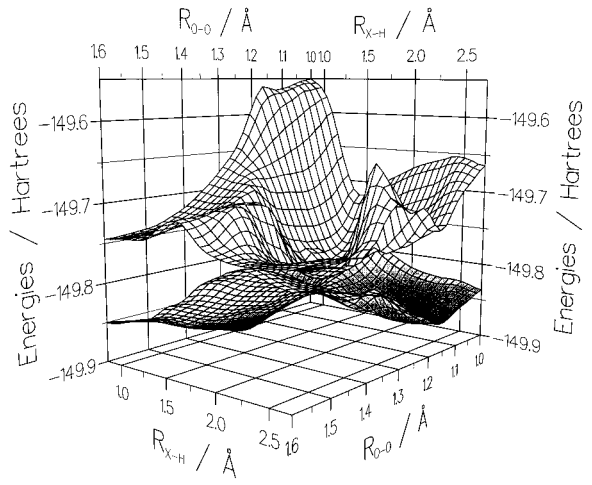

Figure 8. 2D-PESs for the first two roots at a fixed angle $\Theta = 89.8$ degrees.

parameters fully describe the motion of the isolated protonated molecule as they vary in a C_s symmetry space. By keeping the R_{O-O} distance at equilibrium value and by varying R_{O-H} between 0.50 and 2.50 Å (with Θ varying between 30 and 110 degrees) we obtain the PES of Figure 5 which clearly shows the conical topology of the two surfaces. A qualitative analysis based on the character of the surfaces,[22] as performed by us in our previous work,[23] shows clearly, albeit without rigorous proof, that the two surfaces exchange their characters and that we are in the presence of a conical seam even if the multidimension−spline transformation avoids the conical peak because of the lack of convergence next to a degeneracy. In fact, following the gradient of one surface in any chosen direction that crosses the conical point we will avoid the discontinuity only by crossing into the other surface. The same procedure could be followed for the curves of C_{2V} symmetry shown in Figure 2 where, following point-by-point the lower eigenvalues between the two 1D-PES we encounter a discontinuity of the first type in the lower curve, where the latter changes abruptly its symmetry. In other words, we can say that if a potential energy curve (PEC) was previously found to be of a definite polarity,[22] after the crossing one finds that it has changed polarity by going from the attractive to the repulsive behavior or vice versa.

The next step in our work has been to relax the R_{O-O} distance as represented in Figure 6, where on the left column we show the R_{O-H} projections of the PESs and on the right column the Θ projections: in this way, we can appreciate the effect of the two parameters for different R_{O-O} and thereby obtain the three coordinates of the seam points. By stretching the R_{O-O} distance from shorter to larger values, we see that the crossing point gradually moves along R_{O-H} and is more or less constant on the Θ angle. If we now keep these coordinates of Figure 6 and, using further calculations not discussed here for the sake of brevity, we can build the geometries represented in Figure 7 where we see that the seam points found from a full PES of the O_2H^+ belong clearly to the C_{2V} point group. This constitutes a first, albeit qualitative, proof that the seam found previously in C_{2V} symmetry has a conical topology and it represents the preferential *loci* of electron-exchange reaction. To prove the nature of the crossing more unequivocally, we will turn in the next paragraph to the geometric phase of the MCSCF wave function by analyzing its change of sign.

The Study of the CI Coefficients

In the previous calculations, we employed an MCSCF wave function where for "character" of the total wave function ψ we meant the polarity of the ϕ_ith configuration which has the greatest CI coefficient, c_i. Even when we actually performed calculations with about 850 CSFs, only two or three configurations turned out to be important to describe the two interacting electronic terms. In the lower panel on the left of Figure 2 we represented the CI coefficients for the electronic terms of the upper left panel of the same figure, reporting with continuous lines the coefficient of the $^3B_1$ PES and with dashes the coefficients of the other surface. The labeling (2220 2 + 0 2 +) indicates the corresponding configuration of C_{2V} symmetry: $...5a_1^2 6a_1^2\ 1b_1^2 2b_1\ 1b_2^2 1a_2^{24}$ and is the same for the other configurations. The change of character that we can see for the $^3B_2$ happens with an upper root, and it is not seen as being abrupt only because of the spline smoothing that we performed to describe the lack of convergence in that region. This panel confirms the fact that the two curves are of different IRs and cross each other even if the lower state is represented in the "attractive" region by the $^3B_1$ IR and in the "repulsive" region with the $^3B_2$ IR, hence changing character at the crossing point. If we slightly move the approaching direction by getting into the C_s symmetry as represented in Figure 1, at an angle with the oxygen−oxygen direction of $\Theta = 89.8$ degrees, we see that although the point group symmetry is changed, the values of the parameters are very similar to the previous ones and we find similar PECs. In fact, the potential curves depicted in Figure 2 (on the right upper panel) are identical to the previous ones, albeit of different symmetry, as required by a sort of electronic continuity: the curves for the open-shell O_2H^+ are now of the A″ IR and they avoid each other because of the non-crossing rule. Furthermore, when relaxing the R_{O-O} distance but keeping the angle Θ at 89.8 degrees, we obtain the PESs of Figure 8 which are very similar to the ones of Figure 3. A way to see it is to think of the PESs as Riemann surfaces which we cut where they exchange their characters and then sew one surface to the other along this cut in such a way that the new hypersurface never changes character. We should remember, however, that the PESs are similar but essentially different because the PESs of Figure 8 have conical topology and the overlapping of the PESs of Figure 3 can never be of this type, thereby showing that each symmetry induces a specific topology at the crossing.

Looking at the CI coefficients for the configuration (2222 +00 2+), i.e., $...5a'^2 6a'^2 7a'\ 1a''^2 2a''$ orbital representation for both the interacting roots we can see that at short R_{X-H} distances this configuration describes well the upper state, and then

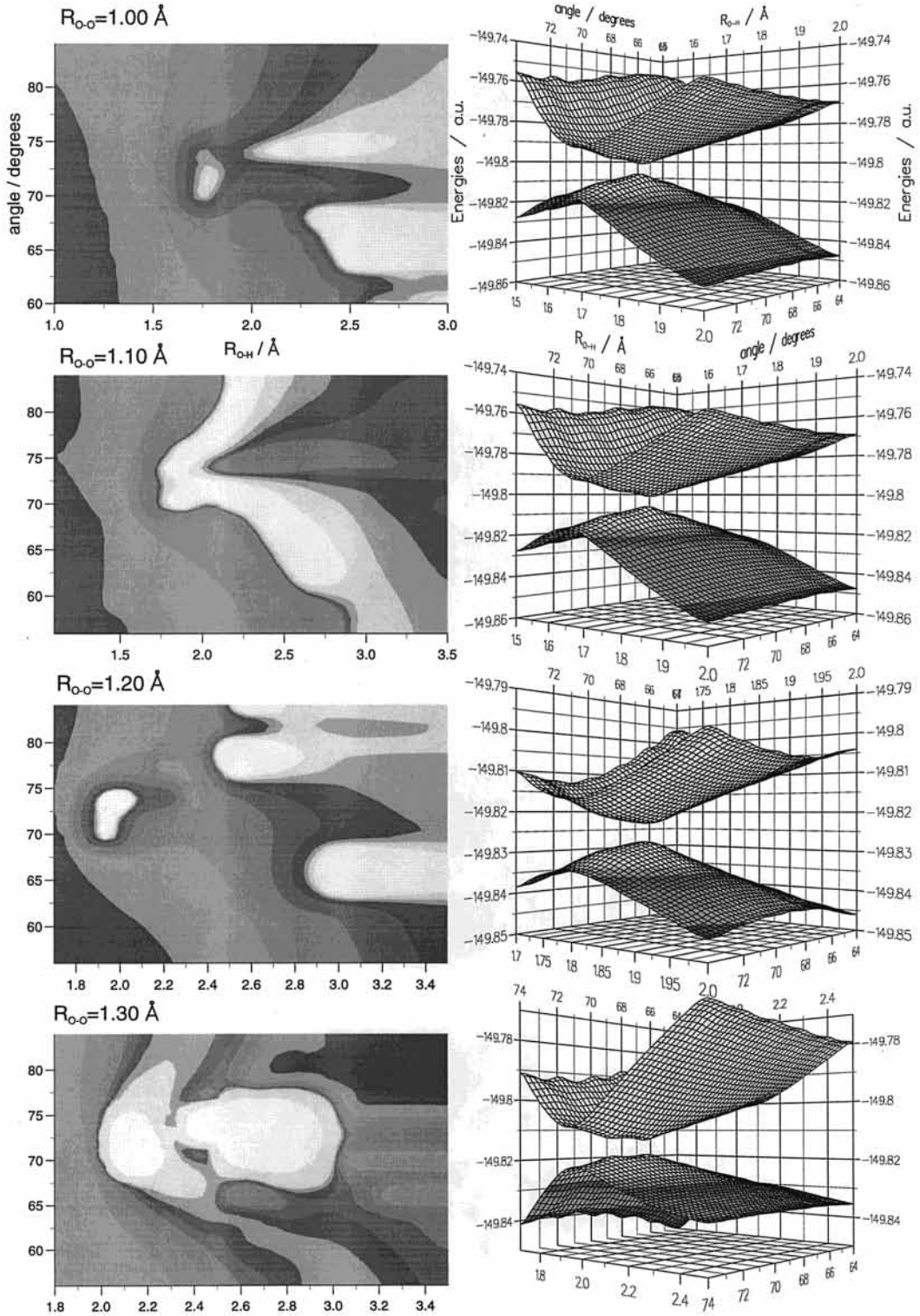

Figure 9. PESs on the right column and related MCSCF-CI coefficients contour plot values of the c_i on the left for different values of relaxing R_{O-O} parameter.

abruptly, at the point of avoided crossing, it describes the lower one. At larger R_{X-H} values, there is another change of sign because we have frozen the R_{O-O} distance. This fact proves that we need to vary all the parameters to have a definitive change of sign in the wave function. However, if we look at this change of sign for different R_{O-O} unidimensional cuts and keep the parametric values at each cut, we obtain the C_s square points of Figure 4 which are close to the C_{2V} seam points as can be seen from their projection of the parametric space. In this way, i.e., by using the electronic continuity criteria, we show that the seam points previously found in C_{2V} symmetry have a conical topology. For a full view of the problem, we need to calculate the MCSCF-CI coefficients by varying all parameters as was done in Figure 9 and Figure 10. On the left column of these figures, we represent contour plots of the MCSCF-CI coefficients and on the right column, the PESs at the same values of R_{O-O}. By taking into account the fact that the white regions of the contour plots are of opposite sign of the black ones, we encounter many isles of changed sign. In fact, as can be seen from the comparison of the last panels of Figure 10 and the

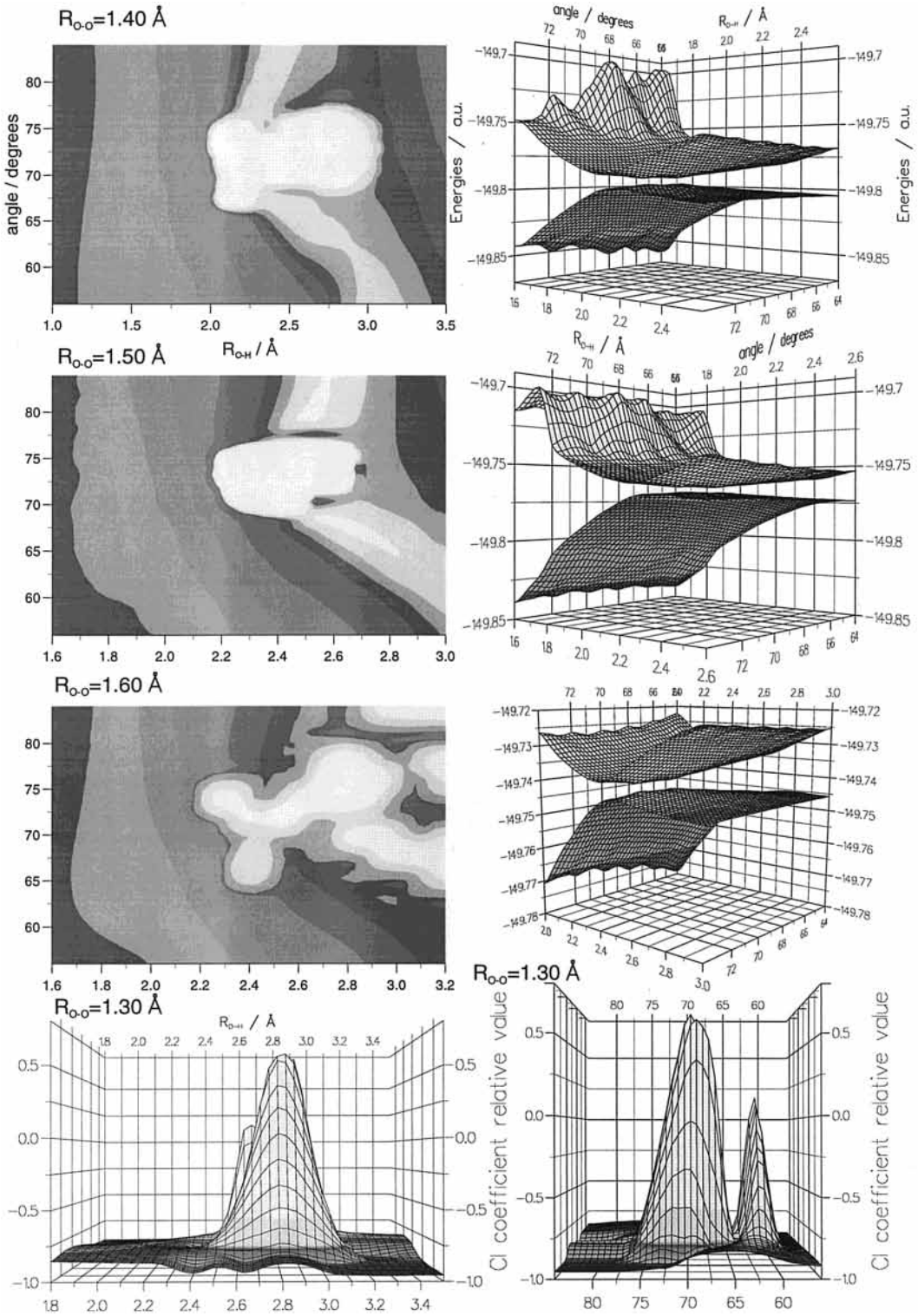

Figure 10. PESs on the right column and MCSCF-CI coefficients on the left column for different values of the R_{O-O} parameter; the lower panels are the 3D representations of the lower panel on the left in Figure 9 from orthogonal points of view.

lower panel on the left of Figure 9, the white regions are of opposite sign than the black regions and the discontinuity is hidden because of the multidimensional spline transformations. An overview of both Figures 9 and 10 allow us to elaborate a 3D path of integration of the geometric phase to have a net change of sign, thereby definitely proving the conical topology of the C_{2V} seam. Furthermore, since we need all the parameters to prove such a feature, we conclude that the **P** space is not separable as previously seen for the **R** space and that P_{O-O} vector is strongly coupled with the other momenta. In other words, the incoming kinetic energy of the proton will be rapidly distributed among the internal modes of the oxygen target which can in turn be strongly coupled with the other external modes via the conical seam. This translational-to-internal energy transfer implies that the dynamic could form at specific energies a collisional complex that can give rise to the well-known Feshbach resonances. These conclusions are in perfect agreement with the results obtained by Sidis et al. with actual dynamical studies.[25] All these considerations suggest that the protonated oxygen could be produced in the ionosphere and as

a stable moiety (the proton affinity of the molecular oxygen is $\mathbf{PA}_{O_2} = 4.38\ eV$[26]).

Conclusions

This work has allowed us to show some interesting features of the conical seams in a specific three-particle system. In the first instance, it has become clear that, to understand the nature of the degeneracies in the C_{2V} symmetry, we need to break the symmetry and study the C_s PESs to appreciate the presence of the gauge transformations induced by the Born−Oppenheimer approximation. In the second instance, we can make a comparison between the seam so found and the conical intersections reported in our previous work[23] for a four-particle case, where the small couplings between the proton and the ozone internal modes in the **P** space allowed us to study the problem in a reduced 2D space. However, the main difference there is that in the ozone case we found a conical intersection without any apparent-symmetry breaking by continuously varying parameters within a C_s symmetry space. We think, in fact, that the avoided crossing obtained from the cut of the multidimensional PES of the protonated ozone and calculated along the C_{2V} axis excludes symmetry-induced conical intersections and therefore forces the system to transfer the charge only via an "electronically induced" conical intersection. On the other hand, for O_2H^+ we have not found any trifurcation point[27] of the C_{2V} seam since no C_s seam is present here. This is in contrast with what was found to happen for systems such as AlH_2,[28] CH_2,[29] O_3,[30] or BH_2. To our knowledge, this is the first time that a molecule of the AB_2 type does not present a double diabolical point.[27] As a third feature, we are able here to compare symmetry versus electronically induced conical intersections: for each type of degeneracy we have, as a global condition, that $\nabla \times \mathbf{A} \neq 0$, a feature that induces a non-negligible geometric phase. We also understand from the general literature that the electronic structure, and consequently the electronically induced degeneracy, provides a more general symmetry condition for a conical seam which is not explicitly shown by the symmetry changes of the nuclei in the **R** spaces, but which is really embedded into the structural properties of the **r** space and cannot be directly brought to the fore by point-group symmetry considerations only. In fact, if moieties such as Li_3[31] and H_3[32−37] present a conical seam in the D_{3h} space because of the degeneracy of the involved IRs of the C_{2V} subgroup, it is also well-known that other moieties such as LiNaK[38] present instead conical seams that are not the exact analogue of that shown by isoatomic moieties because of their different atomic components. The latter, electronically induced conical seams show dominance of the electronic structure of the molecule irrespective of the symmetry and therefore point out the importance of the detailed analysis of the electronic features of the PESs as opposed to the more macroscopic symmetry group analysis.

Acknowledgment. Research grants from the Italian National Research Council (CNR), from the Italian Ministry for University and Research (MURST), and from the Research Committee of the University of Rome are all gratefully acknowledged.

References and Notes

(1) Stevenson, D. P.; Schissler, D. O. *J. Chem. Phys.* **1958**, *29*, 282.
(2) Ding, A.; Henglein, A.; Bunsen-Ges., Ber. *Phys. Chem.* **1969**, *73*, 562.
(3) Lindinger, W.; Albritton, D. L.; McFarland, M.; Fehsenfeld, F. C.; Schmeltekopf, A. L.; Ferguson, E. E. *J. Chem. Phys.* **1975**, *62*, 4101.
(4) Maham, B. H. *J. Chem. Phys.* **1971**, *55*, 1436.
(5) Adams, N. G.; Smith, D. *Chem. Phys. Lett.* **1984**, *105*, 604.
(6) Kim, J. K.; Theard, L. P.; Huntress, W. T., Jr. *Chem. Phys. Lett.* **1975**, *32*, 610.
(7) Ress, M. H. in *Physics and Chemistry of the Upper Atmosphere*; Cambridge Atmospheric and Space Science Series, Cambridge University Press, 1989.
(8) Knowles, P. J.; Werner, H. J. *J. Chem. Phys.* **1985**, *82*, 5053.
(9) Knowles, P. J.; Werner, H. J. *Chem. Phys. Lett.* **1985**, *115*, 259.
(10) Knowles, P. J.; Werner, H. J. *Chem. Phys. Lett.* **1988**, *145*, 514.
(11) Knowles, P. J.; Werner, H. J. *J. Chem. Phys.* **1988**, *9*, 5803.
(12) Werner, H. J. *Adv. Chem. Phys.* **1987**, *59*, 1.
(13) Robbe, J. M.; Monnerville, M.; Chambaud, G.; Rosmus, P.; Knowles, P. *J. Chem. Phys.* **2000**, *252*, 9.
(14) Senent, M. L. *Mol. Phys.* **1999**, *96*, 1587.
(15) Jackiw, R. *Int. J. of Mod. Phys. A* **1988**, *3*, 285.
(16) Mead, C. A.; Truhlar, D. G. *J. Chem. Phys.* **1979**, *70*, 2284.
(17) Berry, M. V. *Proc. R. Soc. London A* **1984**, *392*, 45.
(18) Yarkony, D. R. *Acc. Chem. Res.* **1998**, *31*, 511.
(19) Neumann, J. von; Wigner, E. P. *Phys. Z.* **1928**, *30*, 73.
(20) Neumann, J. von; Wigner, E. P. *Phys. Z.* **1928**, *30*, 844.
(21) Schneider, F.; Zulicke, L.; di Giacomo, F.; Gianturco, F. A.; Paidarova, I.; Polak, R. *Chem. Phys.* **1988**, *128*, 311.
(22) Zener, C. *Proc. R. Soc. A* **1932**, *137*, 696.
(23) Ceotto, M.; Gianturco, F. A. *J. Chem. Phys.* **2000**, *112*, 5820.
(24) Ceotto, M.; Gianturco, F. A. *J. Phys. Chem. A* **1999**, *103*, 9984.
(25) Grimbert, D.; Sidis, V.; Cobout, V. *J. Chem. Phys.* **1998**, *108*, 6331.
(26) Bohme, D. K. in *Interactions Between Ions and Molecules*; P-Ausloos, Ed., Plenum: New York, 1975.
(27) Yarkony, D. R. *Theor. Chem. Acc.* **1997**, *98*, 197.
(28) Chaban, G.; Gordon, M. S.; Yarkony, D. R. *J. Phys. Chem. A* **1997**, *101*, 7953.
(29) Matsunaga, N.; Yarkony, D. R. *J. Chem. Phys.* **1997**, *107*, 7825.
(30) Atchity, G. J.; Ruedenberg, K.; Nanayakkara, A. *Theor. Chem. Acc.* **1997**, *96*, 195.
(31) Gerber, W. H.; Schumacher, E. *J. Chem. Phys.* **1978**, *69*, 1692.
(32) Varandas, A. J. C.; Yu, H. G. *J. Chem. Soc., Faraday Trans.* **1997**, *93*, 819.
(33) Varandas, A. J. C.; Xu, Z. R. *J. Chem. Phys.* **2000**, *112*, 2121.
(34) Wu, Y. S. M.; Kuppermann, A.; Lepetit, B. *Chem. Phys. Lett.* **1991**, *186*, 319.
(35) Longuet-Higgins, H. C.; Opik, U.; Pryce, M. H. L.; Sack, R. A. *Proc. R. Soc. London, Ser. A* **1958**, *244*, 1.
(36) Longuet-Higgins, H. C. *Adv. Spectrosc.* **1961**, *2*, 429.
(37) Child, M. S.; Longuet-Higgins, H. C. *Faraday Discuss. Chem. Soc.* **1963**, *35*, 77.
(38) Varandas, A. J. C.; Tennyson, J.; Murrell, J. N. *Chem. Phys. Lett.* **1979**, *61*, 431.